

The combined role of distance and frequency travel restrictions on the spread of disease

Cate Heine*,¹ Kevin P. O’Keeffe,¹ Paolo Santi,^{1,2} Li Yan,¹ and Carlo Ratti¹

¹*Senseable City Lab, Massachusetts Institute of Technology, Cambridge, MA 02139*

²*Istituto di Informatica e Telematica del CNR, Pisa, ITALY*

Travel restrictions have often been used as a measure to combat the spread of disease—in particular, they have been extensively applied in 2020 against coronavirus disease 2019 (COVID-19). How to best restrict travel, however, is unclear. Most studies and policies simply constrain the distance r individuals may travel from their home or neighbourhood. However, the epidemic risk is related not only to distance travelled, but also to frequency of contacts, which is proxied by the frequency f with which individuals revisit locations over a given reference period. Inspired by recent literature that uncovers a clear universality pattern on how r and f interact in routine human mobility [1, 2], this paper addresses the following question: does this universal relation between r and f carry over to epidemic spreading, so that the risk associated with human movement can be modeled by a single, unifying variable $r \cdot f$? To answer this question, we use two large-scale datasets of individual human mobility to simulate disease spread. Results show that a universal relation between r and f indeed exists in the context of epidemic spread: in both of the datasets, the final size and the spatial distribution of the infected population depends on the product $r \cdot f$ more directly than on the individual values of r and f . The important implication here is that restricting r (where you can go), but not f (how frequently), could be unproductive: high frequency trips to nearby locations can be as dangerous for disease spread as low frequency trips to distant locations. This counter-intuitive discovery could explain the modest effectiveness of distance-based travel restrictions [3] and could inform future policies on COVID-19 and other epidemics.

To test the effects of distance (r) and frequency (f) based travel restrictions, we start with large-scale datasets of individual human movements in New York City and Dakar, Senegal. The datasets each consist of a set of trips \mathcal{T} for N individuals over different time periods T , where each trip indicates a given individual moving between two locations. We then use an agent based SEIR model calibrated with estimates for COVID-19 [4] to simulate disease spread as agents follow the trajectories in our datasets. Aside from their unique trajectories, each individual was assumed identical. In each simulation, we vary two parameters: the maximum travel distance r , measured relative to each agent’s home location

(where the agent’s home was estimated as the most visited location of the agent, see Methods for details), and the travel frequency f , the number of times each location was visited. In practice, this means discarding any trip of length greater than r and all but f randomly selected trips to a given location from our datasets. The details of the spatial partitionings used as well as other simulation details are given in the Methods.

Figures 1(a) and (b) plot the final epidemic size ψ versus travel distance r for different travel frequency f ’s for each dataset after simulations were run over the entire length of the datasets (14 days for the Dakar dataset; 28 days for New York City) with 10,000 agents and a 5% initial infected population. The trends are intuitive and not surprising. For a given f , ψ increases monotonically with r : the further people are allowed travel, the bigger the epidemic. Similarly, for a given r , ψ increases monotonically with f : more frequent trips leads to bigger epidemics. What is surprising, however, is that the $\psi(r)$ curves for each f have similar shape. This echoes a previous finding [1, 2] and hints that ψ , r and f might have a hidden, simple relationship. Figures 1(c) and (d) show that they do. Under the rescaling $r \rightarrow r \cdot f$ all the data appear to merge, as if collapsing to a single, universal curve depending on the unifying factor $r \cdot f$. This curve can be empirically characterized as

$$\psi(r \cdot f) = \frac{L}{1 + e^{a(r \cdot f - b)}}$$

where L , a , and b vary across cities and model types. Figure 2 shows the same scaling collapse is achieved when the SI and SIR models are used, and Figure 7 in the SM shows it persists for different values of the disease parameter R_0 . Taken together, these findings suggest the $r \rightarrow r \cdot f$ scaling collapse is indeed universal, holding true over a wide range of datasets and disease processes.

The discovery of a universal $\psi(r \cdot f)$ curve is unexpected. Recall the complexity of the system we are modeling: a nonlinear, spatially extended disease process coupled to real-world human movements at scales large in space (city scale) and time (several weeks). Even when uncoupled, each of these processes is complicated. Disease transmission across space is known to behave non-trivially [5–8], while human movements likely depend on a tangle of factors such as the distribution of agents homes and workplaces, the subjective nature of human route choices – shortest paths between locations, for instance, are rarely followed [9] – as well as weather and other environmental conditions. Moreover, there is

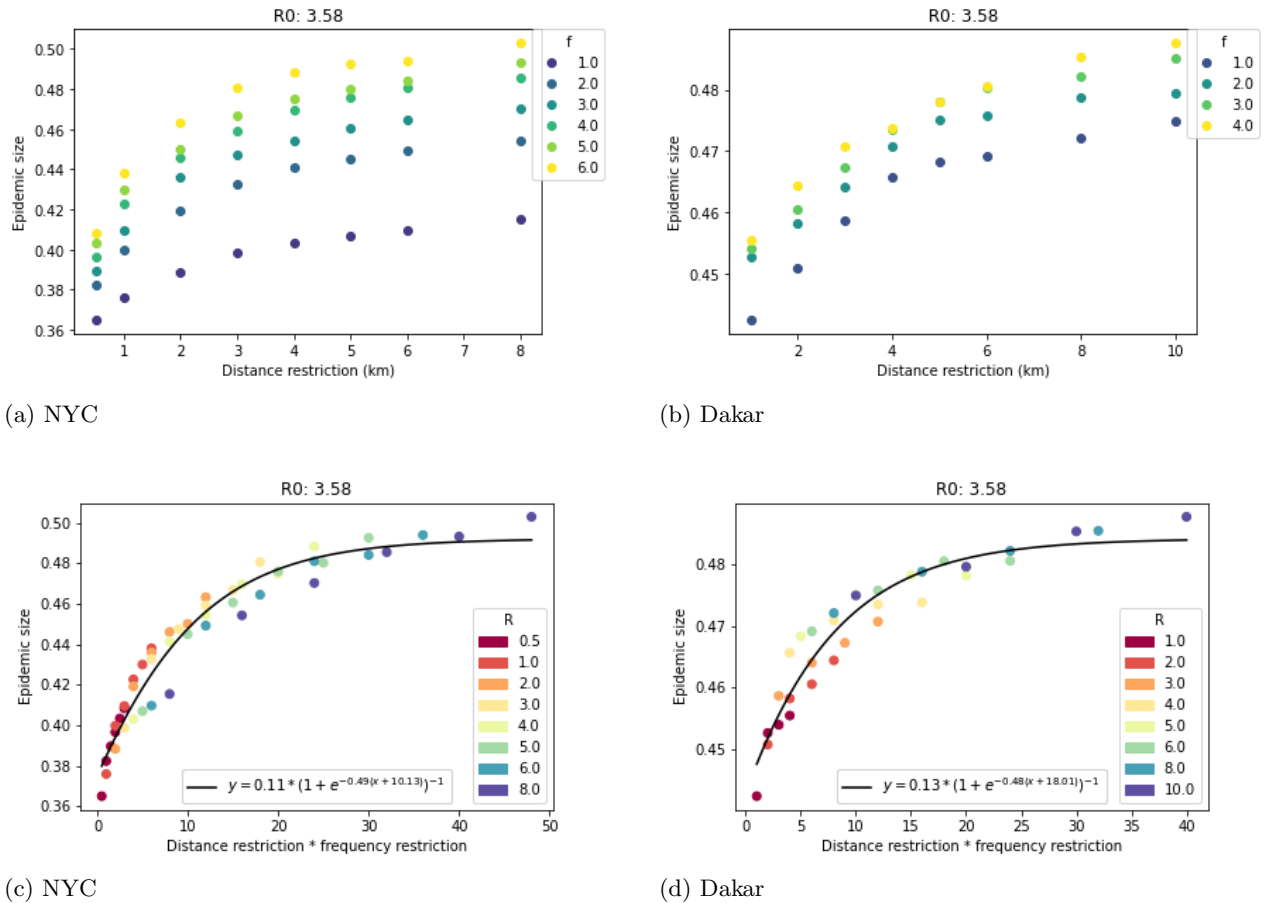


FIG. 1: **Epidemics sizes for SEIR model.** Top row: plots of epidemic sizes versus maximum allowed travel distance r for different max travel frequency f . Bottom row: top row plotted versus $r \cdot f$. As can be seen, there is a universal scaling collapse. Each data point is the average of 5 simulations. For other simulation details see Methods. R^2 values for best-fit lines are .951 (NYC) and .919 (Dakar). Best-fit line parameters are $L = 0.11, a = -0.49, b = 10.13$ (NYC) and $L = 0.13, a = -0.48, b = 18.01$ (Dakar).

no reason to expect each of these influences to movement to be the same in every city. New York and Dakar are hugely different at a number of levels (population size, spatial extent, culture, weather, economics). Yet the $\psi(r \cdot f)$ curve proves that these tremendous complexities that are at play when a disease infects a city somehow produce simple, universal behavior.

After observing the universal relationship between $r \cdot f$ and epidemic size, we check whether there is a relationship between $r \cdot f$ and spatial dispersion of the disease. We analyze the spatial concentration of infected persons in our New York City simulations using the M function developed by Marcon and Puech, which is calculated as a function of some radius k around each agent[10]—see Methods for a detailed description of this statistic. High M indicates tighter clusters of cases; low M indicates a more homogeneous distribution of cases across space. We find that for a given radius k , as r and f increase, $M(k, r, f)$ decreases: infections become consistently more dispersed across the city (see Figure 3a for this relation-

ship when $k = 700\text{m}$). As with epidemic size, under the rescaling $r \rightarrow r \cdot f$, this relationship collapses to a single curve, as shown in Figure 3b. This relationship is robust to the choice of k —as k increases, $M(k, r, f)$ decreases (as would be expected—the larger radius you look at around an agent, the more representative sample of the whole population you will capture) but stays significant and maintains its relationship to $r \cdot f$. This relationship is demonstrated visually in Figures 3c and 3d. When r is fixed at 8, increasing f from 1 to 6 has a clear effect on the extent to which infections spread across the city (Figure 3c); while significant portions of the city remain untouched by infection when $f = 1$, many more grid cells contain at least one infection when $f = 6$. This indicates that restricting $r \cdot f$ is more effective at containing geographic spread of disease than restricting r alone, just as it is effective at containing epidemic size. In Figure 3d, on the other hand, we see that when $r \cdot f$ is held fixed at 12, spatial distribution of infection rates is almost identical for different r and f values, demon-

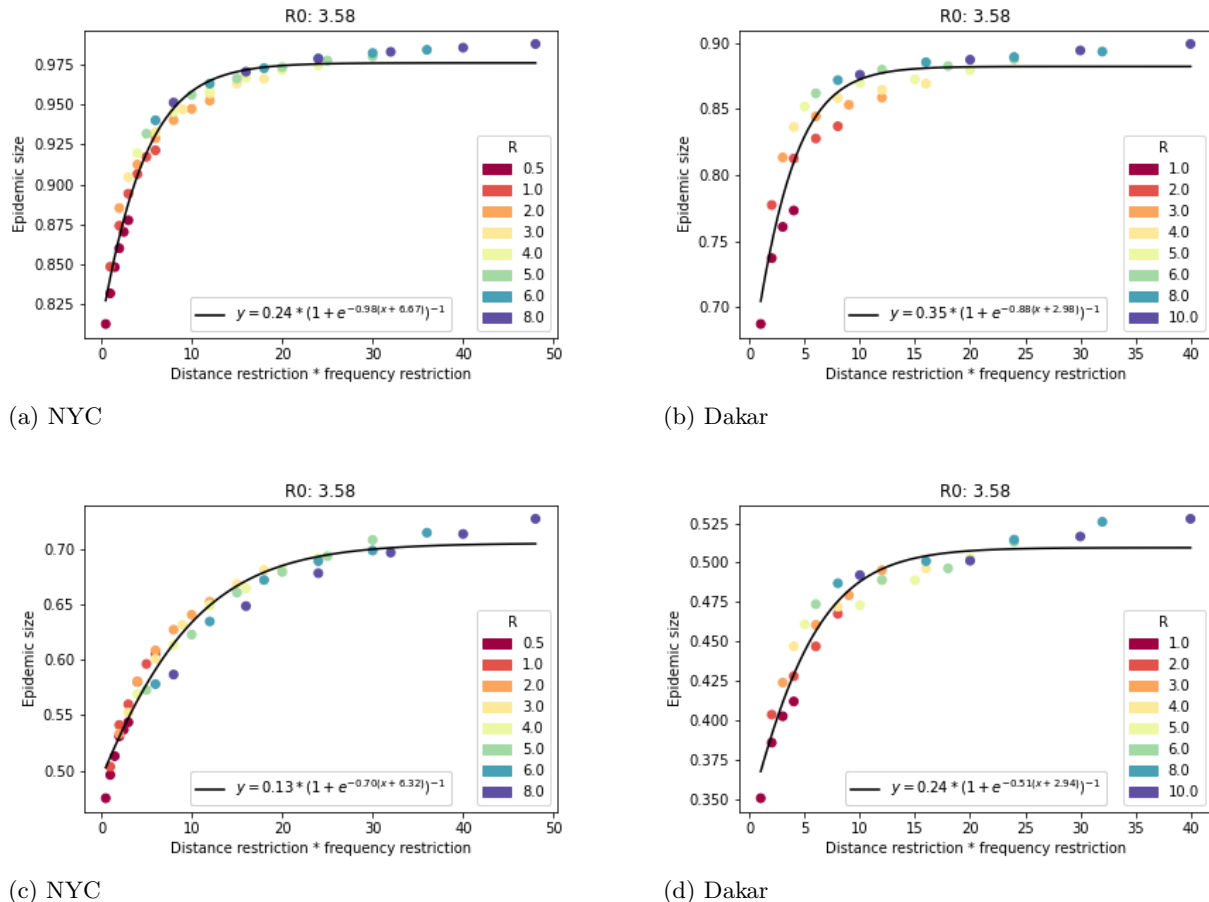


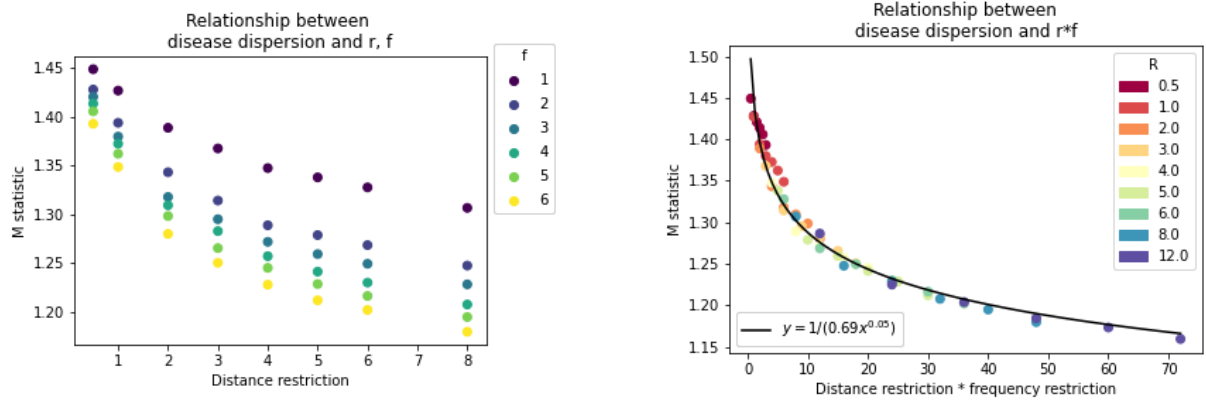
FIG. 2: **Universal scaling collapse in SI and SIR model.** Top row: scaling collapse for SI model. R^2 values for best-fit lines are, from left to right, .970 and .896. Best-fit line parameters are $L = 0.24, a = -0.98, b = 6.67$ (NYC) and $L = 0.35, a = -0.88, b = 2.98$ (Dakar). Bottom row, scaling collapse for SIR model. R^2 values for best-fit lines are, from left to right, .969 and .937. Best-fit line parameters are $L = 0.13, a = -0.70, b = 6.32$ (NYC) and $L = 0.24, a = -0.51, b = 2.94$ (Dakar).

strating the relationship between spatial distribution and $r \cdot f$.

An important implication of the universal $\psi(r \cdot f)$ curve is that short, high frequency trips spread as much disease as long, low frequency trips. In plain English, multiple trips around your neighbourhood are as bad for public health as a single trip to the city center. This is interesting academically, but more importantly, it has implications for policy. It means that restricting travel distance r , but not travel frequency f , could be unproductive – it is not enough to restrict r , the product $r \cdot f$ must be restricted. Consider the drop in epidemic size with distance restriction r and visitation frequency f , $\Delta\psi(r, f) := \psi(r \rightarrow \infty, f \rightarrow \infty) - \psi(r, f)$. When frequency restrictions are ignored in the SI model in NYC, $\Delta\psi(r = 2, f \rightarrow \infty) \approx .44$. When frequencies are restricted this drops to $\Delta\psi(r = 2, f = 2) = .37$. Under frequency-blind policies this considerable reduction in ψ is missed. An upside to the $r \cdot f$ invariance, however, is that strict distance restrictions may be unnecessary.

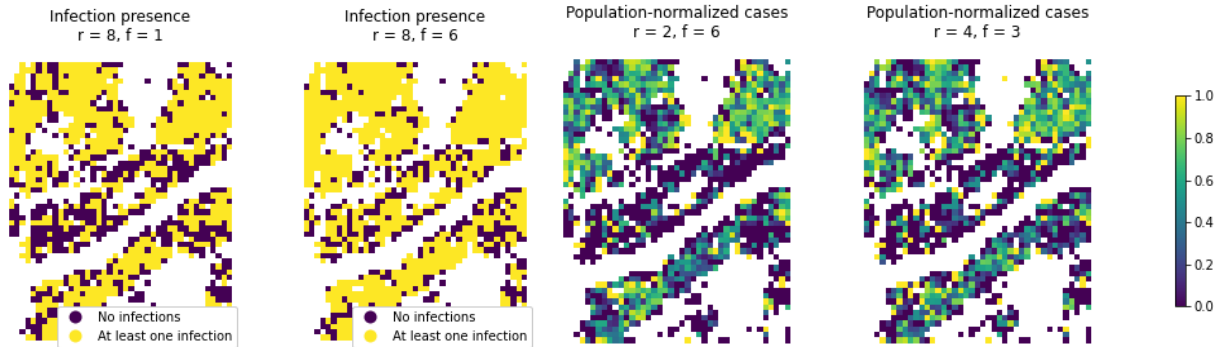
A loose distance restriction (large r) may be offset by a tight frequency restriction (small f) because the transformation $r \rightarrow kr, f \rightarrow f/k$, leaves the product $r \cdot f$ – and thus the epidemic size ψ – unchanged.

Why is the product $r \cdot f$ distinguished? We define $d \propto rf$ as effective travel distance. The significance of d was revealed in recent work [1, 2] on human mobility patterns which shows the number of people who visit a given location f times from a distance r during a certain reference period follow a universal, inverse square law $N(r, f) \propto 1/(rf)^2 \propto 1/E^2$. We suspect the universal $\psi(rf)$ curve found in this paper derives from this inverse square law. Figure 5 tests this intuition by replacing the real-world mobility patterns \mathcal{M}_{real} with the preferential return model [11], a popular and accurate model of human movements faithful to the above distribution of effective travel distance, and a Levy flight, which is not faithful to it [1, 12]. As seen, panel (a) shows a scaling collapse while panel (b) does not. This suggests the universality in $\psi(rf)$ is rooted in the universal inverse



(a) Relationship between frequency restriction and dispersion for radius = 700m.

(b) Scaling collapse for radius = 700m. R^2 value of best-fit line is .97.



(c) Holding r constant but restricting f , we can see that loosening restrictions on f increases spatial dispersion of infections—when f is at 1 (left), infections reach 59.0% of grid cells; when f is relaxed to 6 (right), infections reach 73.8% of grid cells.

(d) In the simulations above, r and f are individually different but $r \cdot f$ is the same. The similar spatial distribution of infections in the two simulations reflects the scaling collapse in dispersion of infection: dispersion depends on $r \cdot f$ as opposed to just r or f . Here, color represents proportion of the grid cell population that is infected at the end of the simulation.

FIG. 3: Universal scaling collapse of spatial dispersion of infections. Like ψ , spatial dispersion M shows a universal scaling collapse with the product $r \cdot f$, as demonstrated in panels (a) and (b). Here, M is calculated using a radius of $k = 700$ meters. This is visually represented in panel (c), where we see the final spatial distribution of infections for two simulations with the same r but different f , and in panel (d), where we see the final spatial distribution of infections for two simulations with the same $r \cdot f$ but different r and f .

square law in human movement.

Since the universal $\psi(r \cdot f)$ curve – and the policy implications we have drawn from it – depends on the real world mobility data \mathcal{M}_{real} collected in the *absence* of COVID-19, it may not hold during an epidemic in which people are known to move differently. Fortunately, our NYC data extends through some of the COVID-19 outbreak so we are able to examine this. Figure 6 shows that the scaling collapse is not quite as clean when we run our simulations on data from the second half of March 2020— r seems to have a weaker effect in March than it did in February, perhaps because individuals were already restricting their own travel radius due to pandemic-related fears. Still, the scaling collapse generally holds under real movement patterns during the COVID-19 pandemic (March 2020). This means that even with individuals’

self-imposed restrictions during a pandemic, imposing r and f restrictions still has a similar effect, proportional to $r \cdot f$.

Our study has limitations. First, there is the inherent limitation of epidemiological modeling; it is known that the SI, SIR, SEIR and other classic disease models make assumptions which bound their accuracy [13–15]. The estimates for the model parameters likely carry error [16], and we also assumed each agent was identical. Second, the scale of our analysis is restricted to the city-level (because our datasets are collected at this level) and so our findings do not necessarily generalize to the perhaps more important case of country-level and international travel policies.

Nevertheless, we believe our results reveal novel insights that could prove useful for future policies on

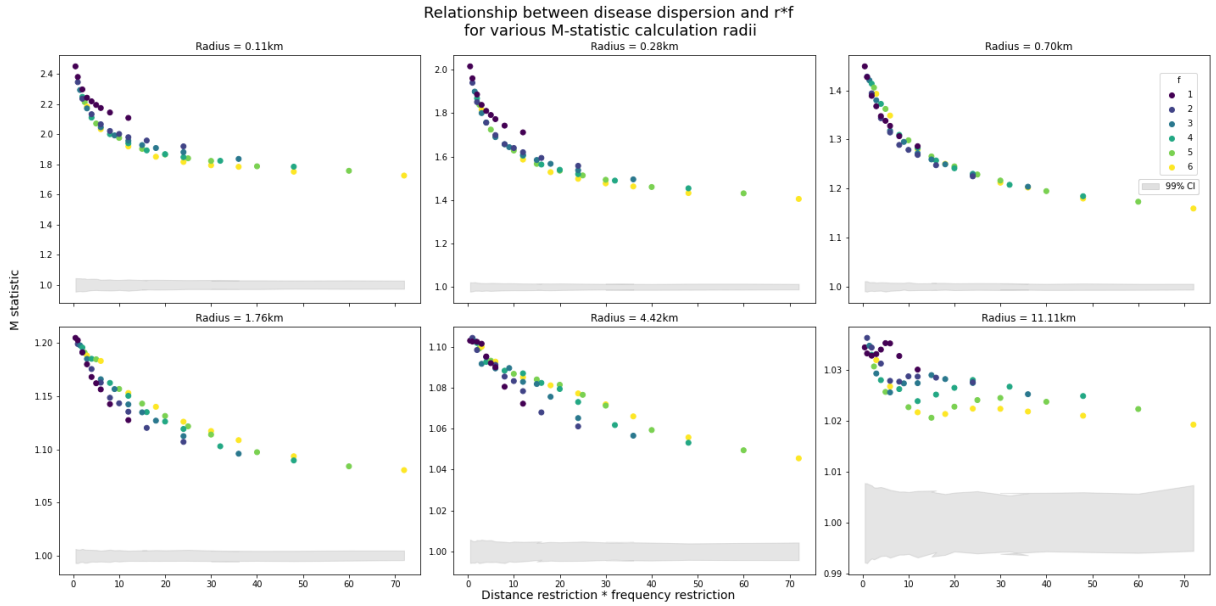
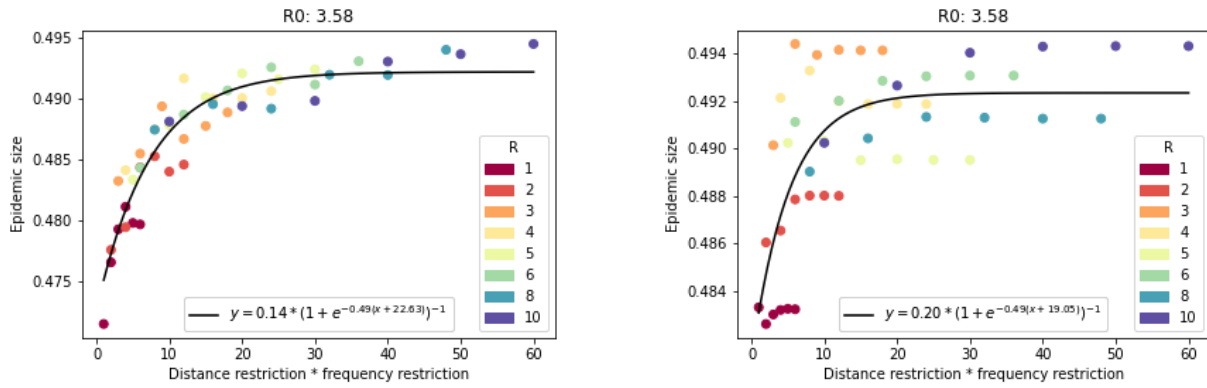


FIG. 4: **Collapse of spatial dispersion of infections for various k .** Spatial dispersion $M(k)$ shows a scaling relationship with $r \cdot f$ regardless of k . 99% confidence bands are shown in gray, indicating that the spatial clustering in infections remains significant across values of $r \cdot f$.



(a) Epidemics sizes for preferential return model. Agents move according to the preferential return model with mobility parameters fitted to Dakar data. 10,000 agents have been used for 2,420 timesteps. Best-fit line $R^2 = .87$

(b) Epidemics sizes for Levy flight model. Agents follow a Levy flight model, drawing distances and times between trips from heavy-tailed distributions fitted to Dakar data. 10,000 agents have been used for 2,420 timesteps. Best-fit line $R^2 = .49$

FIG. 5: **Epidemics sizes for preferential return model (left) and Levy flight model (right).** The preferential return model of mobility captures the relationship between $r \cdot f$ and epidemic size, while the Levy flight model does not.

COVID-19 and other epidemic diseases. As cities and states continue with various levels of lockdown, evidence based policies at the city scale (not to mention the national or international scale) are needed to avoid further waves of infection. Our results directly help this effort. They indicate that the total effective travel distance of a city's inhabitants $d = r \cdot f$ must be bounded – to

bound distance r but not visitation frequency f is a serious blunder. Furthermore, and more optimistically, a bound on travel energies E_{bound} means that strict distance restrictions at the city or town level – as adopted by, e.g., Ireland and Italy at the beginning of the infection – are perhaps unnecessary. Given a desired E_{bound} , a large r can be offset by a small f ; allowing citizens to

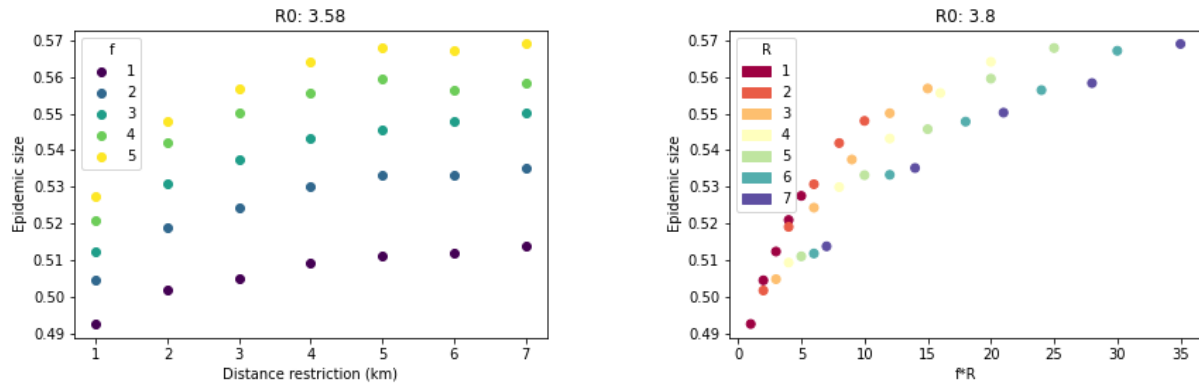


FIG. 6: **Epidemics sizes for NYC during covid outbreak.** Scaling collapse for SEIR model run on March 2020 data.

travel infrequently to distant services (doctors, hospitals etc) may be safe. This inverse relation between travel distance and frequency ($r \propto E_{bound}/f$) could also vitally inform remote working policies. It supports the hypothesis that working from home multiple days per week – and thereby limiting the visitation frequency to workplaces – helps prevent the spread of disease.

Our results may also be useful beyond the city scale, potentially offering some solutions for reopening global travel. If the $r \cdot f$ invariance, or some form of inverse relation between r and f , holds for international mobility patterns, then, as before, lax distance limits could be compensated by strict frequency restrictions. In other words, infrequent international travel may be relatively safe. We acknowledge this is a bold hypothesis, which should be tested in future work. Metapopulation disease models [5, 17, 18], with their convenient trade off between realism and parsimony, seem like a good theoretical starting point for this effort.

ACKNOWLEDGMENTS

The authors would like to thank Allianz, Amsterdam Institute for Advanced Metropolitan Solutions, Brose, Cisco, Ericsson, Fraunhofer Institute, Liberty Mutual Institute, Kuwait-MIT Center for Natural Resources and the Environment, Shenzhen, Singapore- MIT Alliance for Research and Technology (SMART), UBER, Vitoria State Government, Volkswagen Group America, and all the members of the MIT Senseable City Lab Consortium for supporting this research. Research of S.H.S. was supported by NSF Grants DMS-1513179 and CCF-1522054. The authors would also like to thank X-Mode Social, Inc., for provision of the New York City data. We would like to acknowledge ORANGE / SONATEL for providing the data.

AUTHOR CONTRIBUTIONS

C.R. conceived the work. K.P.O. and C.H. designed the simulations. L.Y. acquired the data. C.H. executed the simulations. K.P.O., P.S., and C.H. contributed to writing and revising the manuscript. P.S. and C.R. supervised the research.

DATA AVAILABILITY

The data and code used in this study are available from the authors upon reasonable request and with permission of X-Mode Social, Inc.

METHODS

New York City data. Individuals’ movements in New York City are inferred from GPS traces collected from mobile phones by the company X-Mode over a span of two months (February and March 2020). The raw data contains about 479,163 anonymized users; our analysis uses 10,000 users randomly selected from those that appear in the dataset every day in the month of February.

Dakar data. The Dakar dataset is based on anonymized Call Detailed Records (CDR) provided by the Data for Development (D4D) Challenge. The detailed information of this dataset is provided in [19]. Here, we use the SET2, which includes individual trajectories for 300,000 sampled users in Senegal, and after the preprocess, we have 173,000 users and 173 cells in Dakar region during two weeks of January, 2013. We subselect for users who appear at least 200 times in the dataset to ensure that we have adequate information about their trajectories over the two weeks.

Data preprocessing. The X-Mode data from NYC is

generated on an very fine spatial and temporal scale, with exact latitude and longitude coordinate updates as frequently as every second. The CDR data from Dakar, on the other hand, are generated only for voice calls, text messages or data exchanges and therefore have limited resolution in time. The geographic location of the cell towers and their density determines the accuracy of location measurements through triangularization techniques. Therefore, the trajectories extracted from CDRs constitute a discrete approximation of the moving population $M(x; y; t)$. There are several steps in preprocessing of the data before it can be suitable for use in our analysis, which vary between the X-Mode data and the CDR data.

The main steps for the NYC data are: i) We use density-based spatial clustering of applications with noise (DBSCAN) to group tightly-clustered latitude/longitude pairs in each individual's trajectory into locations. If a cluster of at least five latitude/longitude points exists such that no point is more than .0004 degrees (about 56 meters) from two other points in the cluster, those points are grouped together as a single location. ii) Each agent is assigned the DBSCAN cluster it visits most as its home location. iii) We drop all locations in the trajectory that have been visited for less than a minimum time $\tau_{min} = 15min$. iv) In order to restrict travel distance r , we calculate distance between locations by the haversine formula, which derives the great-circle distance between two points on a sphere. All locations that are more than r km from an agents home location are removed from their trajectory. v) In order to restrict travel frequency f , for each DBSCAN cluster that an agent visits more than f distinct times (where distinct visits are determined by an agent leaving a location and then coming back to it), we randomly select f visits to include in their trajectory and drop the rest.

The main steps for the Dakar data are: i) We view each cell tower as a different location in the city. ii) For each person, we determine the home location as the cell tower location which has been visited for the most cumulative time. By summing over all days in a given time window, one can find the home cell with high level of confidence for the majority of subjects. iii) We drop all locations in the trajectory that have been visited for less than a minimum time $\tau_{min} = 10min$. iv) In order to restrict travel distance r , we calculate distance between cell towers by the haversine formula, which derives the great-circle distance between two points on a sphere. All cell towers that are more than r km from an agent's home location are removed from their trajectory. v) In order to restrict travel frequency f , for each location that an agent visits more than f distinct times (where distinct visits are determined by an agent leaving a location and then coming back to it), we randomly select f visits to include in their trajectory and drop the rest (excepting visits to an agent's home location, which are not restricted).

The duration of stay, frequency, and distance criteria on defining cell visits yields a list of cells visited by

that subject over the study period for a given frequency restriction f and distance restriction r .

Simulation details. We run an agent-based SEIR, SIR, and SI models with $N = 10,000$ agents, 5% of which are initialized to be infected (1% in the SI and SIR Dakar models). Each agent is assigned the trajectory of a real person from our dataset, with location updated every 900 seconds (15 minutes) for the NYC simulations or every 600 seconds (10 minutes) for the Dakar simulations. At each time step, each user's location is updated according to their assigned trajectory and infection status is updated according to the following parameters, drawn from Chen 2020[4]'s estimates of $R_0 = 3.58$, incubation period = 5.2 days, and infection period = 5.8 days:

$$\beta = \text{daily transmission parameter} = \frac{3.58}{5.8} = .617$$

$$\sigma = \text{daily rate at which an exposed person becomes infective} = 1/5.2$$

$$\gamma = \text{daily recovery parameter} = 1/5.8$$

Let s be the number of time steps in a day. We then transform the above daily parameters into timestep parameters as follows:

$$\beta^* = \text{time step transmission probability} = \beta/s$$

$$\gamma^* = \text{time step recovery probability} = 1 - \sqrt[s]{1 - \gamma}$$

$$\sigma^* = \text{time step probability that an exposed person becomes infective} = 1 - \sqrt[s]{1 - \sigma}$$

Finally, let I_{local} and N_{local} be the number of infected agents and total agents within a 190 meter radius of the agent's current location for the NYC data or within the same cell tower location for the Dakar data.

$$\mathbb{P}[S \rightarrow E] = \beta^* * \frac{I_{local}}{N_{local}}$$

$$\mathbb{P}[E \rightarrow I] = \sigma^*$$

$$\mathbb{P}[I \rightarrow R] = \gamma^*$$

In the SIR and SI models, if an agent becomes infected on a given day, they will become contagious at the start of the next day.

Quantifying dispersion. We use the M function developed in [10] to quantify spatial dispersion of disease in our New York City simulations for a given r , f . The M function is calculated as follows: for each infected agent I and some radius k , we calculate the ratio between the proportion of agents within k of I which are infected to the proportion of agents in the total population which are infected. Summing this value over all infected agents I and dividing by $N - 1$, where N is the number of infected agents, gives $M(k)$, the M function evaluated at k . While M is generally analyzed as a function over all reasonable k , we evaluate the M function at a specific k in order to compare spatial dispersion across $r \cdot f$ values at that k , and then show that the relationship is robust to choice of k .

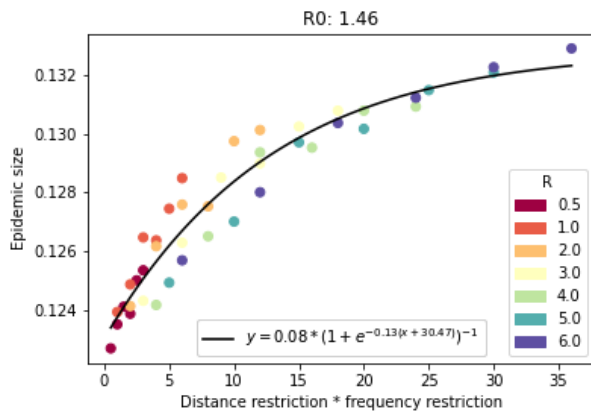


FIG. 7: Epidemics sizes for NYC covid outbreak with lower $R_0 = 1.46$, suggesting the scaling collapse is robust. R^2 of best-fit line is .925.

Confidence intervals for $M(k)$ are obtained by Monte Carlo simulation—for a given epidemic size ψ , we randomly assign ψ infections across the population 1,000 times and calculate M_ψ each time. By taking the .025 and .975 quantiles of these simulated M , we form an upper and lower bound on M_ψ . It is notable that our empirical M never reaches this confidence band, implying

that spatial dispersion is significantly non-homogenous for every k and ψ .

Universality robustness. Here we demonstrate that the universal $\psi(r \cdot f)$ curve is robust to changes in the parameters R_0 by running our simulations with estimated transmission parameters for the 2009 H1N1 influenza strain of $\beta = .913, \gamma = 1.6, \sigma = 1$ [20, 21]. Figure 7 shows that, with these parameters, the $\psi(r \cdot f)$ universality still holds.

Preferential return model. The preferential return model is based off of that proposed in Song et al. [22]. With some probability P_{new} , agents return to a location they have already visited; with probability $1 - P_{\text{new}}$ they visit a new location with distance drawn from the empirical distance distribution and direction drawn uniformly at random. Waiting times between trips are also drawn from the empirical distribution. The probability p is a function of the number of locations already visited:

$$P_{\text{new}} = \rho S^{-\gamma}$$

where S is the number of locations visited. The parameters ρ and γ are fit to the real data using least-squares regression (using the NYC dataset, we find $\rho = .500$ and $\gamma = .267$.)

-
- [1] Dong, L. *et al.* The spectral dimension of human mobility. *arXiv preprint arXiv:2002.06740* (2020).
- [2] Schläpfer, M., Szell, M., Salat, H., Ratti, C. & West, G. B. The hidden universality of movement in cities. *arXiv preprint arXiv:2002.06070* (2020).
- [3] Chinazzi, M. *et al.* The effect of travel restrictions on the spread of the 2019 novel coronavirus (covid-19) outbreak. *Science* **368**, 395–400 (2020).
- [4] Chen, T.-M. *et al.* A mathematical model for simulating the phase-based transmissibility of a novel coronavirus. *Infectious diseases of poverty* **9**, 1–8 (2020).
- [5] Watts, D. J., Muhamad, R., Medina, D. C. & Dodds, P. S. Multiscale, resurgent epidemics in a hierarchical metapopulation model. *Proceedings of the National Academy of Sciences* **102**, 11157–11162 (2005).
- [6] Vespignani, A. Modelling dynamical processes in complex socio-technical systems. *Nature physics* **8**, 32–39 (2012).
- [7] Pastor-Satorras, R. & Vespignani, A. Epidemic spreading in scale-free networks. *Physical review letters* **86**, 3200 (2001).
- [8] Balcan, D. *et al.* Multiscale mobility networks and the spatial spreading of infectious diseases. *Proceedings of the National Academy of Sciences* **106**, 21484–21489 (2009).
- [9] Malleson, N. *et al.* The characteristics of asymmetric pedestrian behavior: A preliminary study using passive smartphone location data. *Transactions in GIS* **22**, 616–634 (2018).
- [10] Marcon, E. & Puech, F. Measures of the geographic concentration of industries: improving distance-based methods. *Journal of Economic Geography* **10**, 745–762 (2010). URL <https://doi.org/10.1093/jeg/1bp056>.
- [11] See the Methods for a description of the preferential return method.
- [12] Chechkin, A., Metzler, R., Klafter, J. & Gonchar, V. *Introduction to the Theory of Lévy Flights*, 129 – 162 (2008).
- [13] Cirillo, P. & Taleb, N. N. Tail risk of contagious diseases. *Nature Physics* 1–8 (2020).
- [14] Donnat, C. & Holmes, S. Modeling the heterogeneity in covid-19’s reproductive number and its impact on predictive scenarios. *arXiv preprint arXiv:2004.05272* (2020).
- [15] Buchanan, B. The limits of a model. *Nature Physics* 1–8 (2020).
- [16] Ma, S. *et al.* Epidemiological parameters of coronavirus disease 2019: a pooled analysis of publicly reported individual data of 1155 cases from seven countries. *Medrxiv* (2020).
- [17] Colizza, V. & Vespignani, A. Invasion threshold in heterogeneous metapopulation networks. *Physical review letters* **99**, 148701 (2007).
- [18] Arino, J. & Van den Driessche, P. Disease spread in metapopulations. *Fields Institute Communications* **48**, 1–12 (2006).
- [19] de Montjoye, Y.-A., Smoreda, Z., Trinquart, R., Ziemlicki, C. & Blondel, V. D. D4d-senegal: The second mobile phone data for development challenge (2014). 1407.4885.
- [20] Biggerstaff, M., Cauchemez, S., Reed, C., Gambhir, M. & Finelli, L. Estimates of the reproduction number

- for seasonal, pandemic, and zoonotic influenza: a systematic review of the literature. *BMC Infectious Diseases* **14**, 480 (2014). URL <https://doi.org/10.1186/1471-2334-14-480>.
- [21] Cori, A. *et al.* Estimating influenza latency and infectious period durations using viral excretion data. *Epidemics* **4**, 132–138 (2012). URL <http://www.sciencedirect.com/science/article/pii/S175543651200031X>.
- [22] Song, C., Koren, T., Wang, P. & Barabási, A.-L. Modelling the scaling properties of human mobility. *Nature Physics* **6**, 818 (2010).